Obstacle Avoidance for Unmanned Aerial Vehicles

Article *in* Journal of Intelligent & Robotic Systems · January 2012

DOI: 10.1007/s10846-011-9587-z · Source: DBLP

2 authors:

Gonçalo Charters Santos Cruz
Portuguese Air Force Academy
17 PUBLICATIONS **91** CITATIONS
SEE PROFILE

Pedro Encarnação
Universidade Católica Portuguesa
124 PUBLICATIONS **1,283** CITATIONS
SEE PROFILE

J Intell Robot Syst (2012) 65:203–217
DOI 10.1007/s10846-011-9587-z

Obstacle Avoidance for Unmanned Aerial Vehicles

Gonçalo Charters Santos Cruz · Pedro Miguel Martins Encarnação

Received: 12 January 2011 / Accepted: 18 April 2011 / Published online: 27 October 2011

Abstract This work is framed within the PITVANT project and aims to contribute to the development of obstacle avoidance techniques for unmanned aerial vehicles (UAVs). The paper describes the design, implementation and experimental evaluation of a potential field obstacle avoidance algorithm based on the fluid mechanics panel methods. Obstacles and the UAV goal position are modeled by harmonic functions thus avoiding the presence of local minima. Adaptations are made to apply the method to the automatic control of a fixed wing aircraft, relying only on a local map of the environment that is updated with information from sensors onboard the aircraft. Hardware-In-Loop simulations show the good performance of the proposed algorithm in the envisioned mission scenarios for the PITVANT vehicles.

G. C. S. Cruz (✉)
Portuguese Air Force Academy, Sintra,
2715-021, Portugal
e-mail: gccruz@academiafa.edu.pt

P. M. M. Encarnação
Faculty of Engineering, Catholic University
of Portugal, Rio de Mouro, 2635-631, Portugal
e-mail: pme@fe.lisboa.ucp.pt

Keywords PITVANT · Obstacle avoidance · UAV · Guidance and control of autonomous vehicles

1 Introduction

The challenge of designing obstacle avoidance systems has been present since the beginning of robotics. This stems from the necessity of creating autonomous robots that are able to avoid unforeseen obstacles in their environment relying only on information gathered by sensors onboard.

The problem was initially approached by Khatib [16] using artificial potential fields to repel wheeled mobile robots from obstacles, while attracting them to a goal position. The major disadvantage of Khatib's method is the possibility of existence of local minima in the potential field, trapping the vehicle. Several attempts were made to overcome this limitation. For example, Barraquand et al. [2] suggested to search the potential field for local minima and add intermediate control points to eliminate those minima. Waydo and Murray [23] used stream functions to derive a two dimensional potential field method free of local minima. They successfully applied the method both to static and moving obstacles.

Borenstein and Koren [3] proposed the so called histogram vector field also for wheeled mobile robots obstacle avoidance. In this technique,

the environment is represented by a Cartesian histogram grid iteratively updated by sensors. The information contained in the grid is then used to compute the direction to be followed by the vehicle. Dynamic Window Approach methods were firstly developed by Fox et al. [12] and then extended by Brock and Khatib [4]. The main advantage of this approach is to consider the dynamics of the robot. The dynamics of the robot is also considered in the technique developed by Lapierre et al. [17], denominated Deformable Virtual Zone (DVZ). However, DVZ methods usually lead to very low vehicle speeds. Alternative obstacle avoidance methods include techniques based on the behavior of animals and humans moving in complex environments [10] and strategies based on neural networks [8].

In the case of Autonomous Underwater Vehicles (AUVs), it is worth mentioning the work developed at the Naval Postgraduate School, Monterrey, CA, USA. Fodrea [11] and Hemminger [14] subdivided the problem, avoiding obstacles in the vertical plane and in the horizontal plane, respectively. Paim et al. [18] applied the DVZ methods to the case of AUVs cruising at fixed depths. Also in the marine environment but with surface vehicles, Carvalhosa et al. [6] used harmonic potential functions to compute obstacle free paths.

Obstacle avoidance methods for Unmanned Air Vehicles (UAVs) differ in accordance to the maneuverability characteristics of the platforms for which they are intended for. While moving wing vehicles, like helicopters or quadrotors, may hover and reverse speed, fixed wing vehicles must fly above the stall speed. The latter thus represent a bigger challenge, aggravated by typical weight and power restrictions, and limits of performance. Scherer et al. [19] proposed a behavioral based obstacle avoidance reactive controller for moving wing aircraft. A strategy based on panel methods was developed by Uzol et al. [21] for fixed wing aircraft. However, they assumed the knowledge of a global map of the environment. Call et al. [5] presented a 2D sliding mode obstacle avoidance controller in the horizontal plane. Griffiths [13] makes use of optical flow to detect obstacles and computes a lateral bias necessary to avoid them. These approaches do not take advantage of the full capabilities of an UAV. Whenever the obstacle configuration in the horizontal plane creates a hazardous situation for the UAV, a strategy to fly over the obstacles should be considered.

None of the above mentioned techniques addresses simultaneously the following desirable characteristics of an obstacle avoidance system for a fixed wing unmanned aerial vehicle: provide 3D avoidance maneuvers, rely only on a local map of the environment iteratively updated from onboard sensor information, take advantage of commercial autopilots increasing safety of operation, and also assure that the vehicle speed stays above the stall speed.

The work here presented is framed within the Research and Technology Project in Unmanned Air Vehicles (PITVANT) led by the Portuguese Air Force Academy (AFA) and the Faculty of Engineering of the University of Porto (FEUP), with the collaboration of the University for Armed Forces Munich, the University of California at Berkeley, the Swedish Defence Research Agency, the University of Michigan, Embraer and Honeywell [1]. The main objectives of this program are: the exploration of small platforms, the development of new technologies and new concepts of operation, with an emphasis on the exploration of cooperative control systems for teams of autonomous aerial, marine and land vehicles. The foremost mission scenario for this project is aerial surveillance, for both military and civilian purposes. In order to accomplish these missions, aircraft should be able to fly at lower altitudes, thus increasing the probability of encountering unforeseen obstacles. To detect obstacles, onboard passive sensors should be used, like vision systems. Fixed wing aircraft have been widely used within the PITVANT project since they are the most appropriate for covering large distances efficiently. However they pose additional challenges on obstacle avoidance algorithms since they must fly at speeds above the stall speed. The obstacle avoidance system here presented is based on the panel methods used in fluid mechanics to describe the motion of a fluid in the presence of obstacles [9]. It resorts to harmonic functions, therefore avoiding the presence of local minima.

The symmetric of the potential field gradient is used as a reference for the direction of the

velocity vector. The aircraft speed is controlled by an onboard autopilot. This autopilot is also responsible for controlling the vehicle dynamics, as well as estimating and counteracting external disturbances, like wind. This inner-outer (dynamics-kinematics) control loop structure is the standard approach for UAV control, taking advantage of the convenience of having a commercial autopilot in the loop (see for example Kaminer et al. [15]). Adaptations necessary to deal only with a local map that is updated iteratively from the onboard sensor information as well as methods for automatically computing algorithm parameters are presented.

The paper is organized as follows: Section 2 describes the standard potential field derivation using panel methods while its particularization for applications to the fixed wing aircraft used within the PITVANT project is provided in Section 3. Section 4 contains a brief description of the Hardware-In-Loop simulation setup for one of the PITVANT UAVs and shows the simulation results obtained with the proposed obstacle avoidance algorithm. Finally, Section 5 presents the conclusions and points out future work.

2 Potential Field Derivation

This section follows closely the exposition in *Autonomous Robots Modeling, Path Planning, and Control* [9].

2.1 Sink

In order to attract the UAV towards its goal, an attractive harmonic potential field is needed. In fluid mechanics this attractive potential is modeled by a singular point sink as

$$\phi_g = -\frac{\lambda_g}{R_g} \ , \tag{1}$$

where $\lambda_g > 0$ is the sink strength and R_g is the distance between the vehicle position (x_1, x_2, x_3) and the goal point (x_{g1}, x_{g2}, x_{g3}). The goal sink potential has spherical symmetry and provides the potential field global minimum. Figure 1 shows the potential field created by a sink located at the origin in different planes.

2.2 Uniform Flow

Despite the attractive nature of the goal sink, the attraction caused by the total potential field can be compromised in areas farther from the goal, where the strength of the sink decays very rapidly. If this happens, the UAV will not reach its objective. In order to create a more effective attractive field, a potential function describing an uniform flow pointing from the start point to the goal and whose intensity decreases linearly is used:

$$\phi_u = -(a_1 x_1 + a_2 x_2 + a_3 x_3) U \ , \tag{2}$$

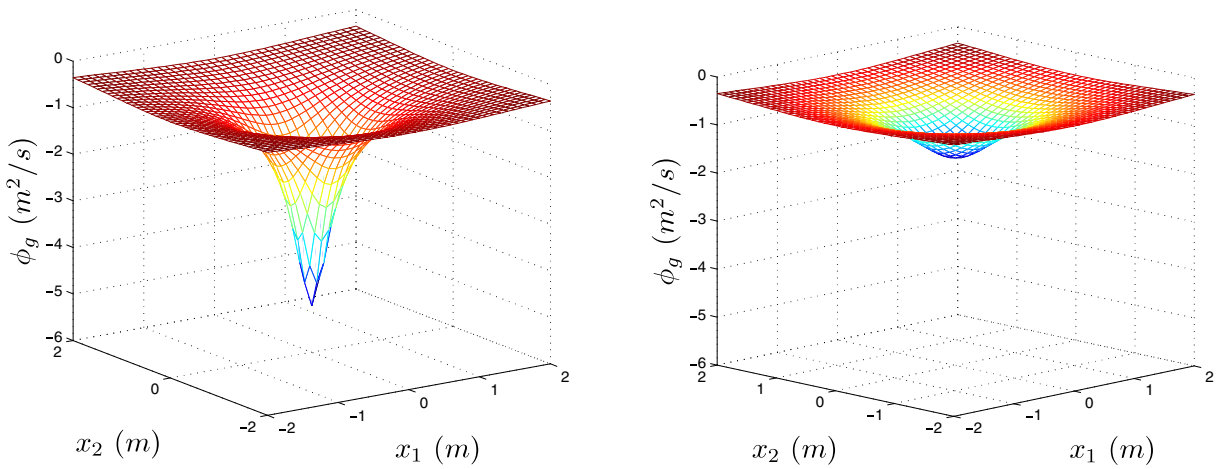

Fig. 1 Potential created on the planes $x_3 = 0.2$ and $x_3 = 0.6$ by a sink located at the origin $x_g = (0, 0, 0)$

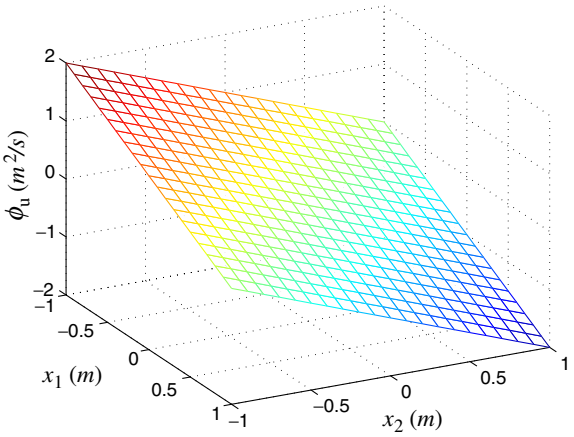

Fig. 2 Potential created on the plane $x_3 = 0$ by a uniform flow with strength $U = \frac{1}{\sqrt{3}}$ m/s

where a_1, a_2 and a_3 are the direction cosines of the vector connecting the start point to the goal point

$$a_1\hat{i} + a_2\hat{j} + a_3\hat{k} = \frac{x_g - x_s}{|x_g - x_s|} \tag{3}$$

($\hat{i}$, $\hat{j}$ and $\hat{k}$ denote the versors of the coordinate system).

The potential caused by a uniform flow on the plane $x_3 = 0$ is displayed in Fig. 2. If the strength U was higher, the gradient of the potential would increase.

2.3 Panel

According to the panel method, obstacles are approximated by polyhedrons whose polygonal faces are modeled by panels that deflect the flow. On each panel j, harmonic sources with strength per unit area λ_j are uniformly distributed. These sources correspond to the symmetric of a sink and they will repel the UAV. The potential in a point $C(x_1, x_2, x_3)$ associated to the panel j with a surface S_j is thus given by

$$\phi_j(x_1, x_2, x_3) = \lambda_j \int_{S_j} \frac{dS_j}{R_j}\ , \tag{4}$$

where R_j is the distance from C to a point on the surface S_j and $\lambda_j > 0$. Details on this integration can be found in Wilton et al. [24]. Figure 3 shows the potential created by a 2 m × 2 m panel parallel to the $x_1 - x_2$ plane and centered at its origin, computed on two different horizontal planes at increasing distances from the panel.

2.4 Harmonic Potential Field

To create the total potential field ϕ for a given configuration, the individual harmonic potential functions are superimposed (see Fig. 4):

$$\phi(x_1, x_2, x_3) = \phi_u + \phi_g + \sum_{j=1}^{m} \phi_j, \tag{5}$$

where m is the number of panels considered.

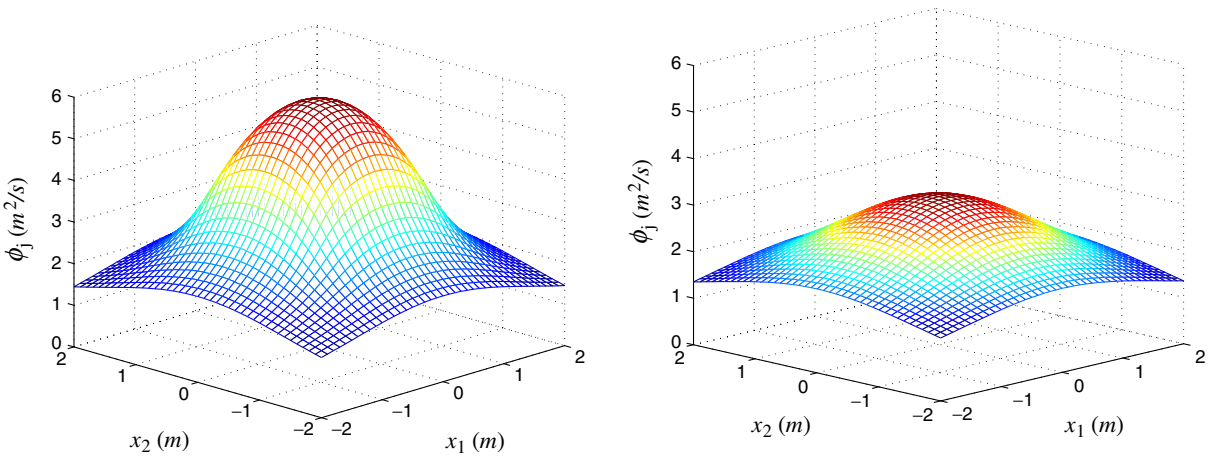

Fig. 3 Potential created by a 2 m × 2 m panel parallel to the $x_1 - x_2$ plane and centered at its origin, computed on two different horizontal planes at increasing distances from the panel

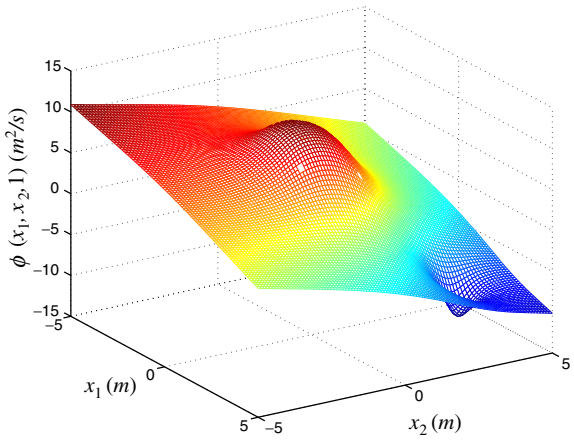

Fig. 4 Harmonic potential field corresponding to the superposition of a sink, an uniform flow and six panels corresponding to a 2 m × 2 m × 1 m quadrangular prism centered at the origin of the axes

The strengths U, λ_g and λ_j must be carefully chosen such that the total potential field has its global minimum at the sink and the attractive effect towards the sink always exceeds the repulsive effect of the obstacles. Defining λ_0 as

$$\lambda_0 = \sum_{j=1}^{m} A_j \lambda_j \ , \tag{6}$$

the sum of the repulsive strengths of all panels weighted by the panels areas, the convergence towards the sink property can be formally posed as

$$-\lambda_g > \lambda_0 > 0 \ . \tag{7}$$

Another condition that should be met is that the velocities

$$V_i = -\frac{\partial \phi_u}{\partial \hat{n}_i} - \frac{\partial \phi_g}{\partial \hat{n}_i} - \sum_{j=1}^{m} \frac{\partial \phi_j}{\partial \hat{n}_i} \qquad i = 1, \ldots, m, \tag{8}$$

where $\hat{n}_i$ is normal to the panel i, must be different from zero and point outwards the obstacle volume at the panels' centers c_i, i.e.,

$$V_i = \frac{\partial \phi}{\partial \hat{n}_i} > 0 \ . \tag{9}$$

This inequality can be used to compute the unknown panel strengths per unit area λ_j after choosing the velocities V_i. However, there's no guarantee that the chosen velocities lead to panel strengths satisfying Eq. 7. Thus, it is more effective to determine the range of velocities V_i for which the resulting panel strengths per unit area λ_j satisfy Eq. 7. Writing the panel intensities as

$$\Lambda = [\lambda_1, \lambda_2, \ldots, \lambda_m]^T \tag{10}$$

and

$$\phi_j = \lambda_j \phi'_j \ , \tag{11}$$

Λ can be determined by

$$\Lambda = P^{-1}(-V + W) \ , \tag{12}$$

where the matrices W and P are given by

$$W = -\frac{\partial \phi_u}{\partial n_i}|_{ci} - \frac{\partial \phi_g}{\partial n_i}|_{ci} = \hat{n}_i \cdot \left(a_1 \hat{i} + a_2 \hat{j} + a_3 \hat{k}\right) - \hat{n}_i \cdot \frac{\lambda_g (x_{ci} - x_g)}{|x_{ci} - x_g|^3}$$
$$i = 1, \ldots, m \text{ and} \tag{13}$$

$$P = \frac{\partial \phi'_j}{\partial n_i}|_{ci} = \hat{n}_i \cdot \left(\frac{\partial \phi'_j}{\partial x_1}|_{ci}\hat{i} + \frac{\partial \phi'_j}{\partial x_2}|_{ci}\hat{j} + \frac{\partial \phi'_j}{\partial x_3}|_{ci}\hat{k}\right)$$
$$i, j = 1, \ldots, m \text{ and} \tag{14}$$

$$V = [V_1, V_2, \ldots, V_m]^T. \tag{15}$$

To minimize the possibility of the potential field being attractive at the periphery of a large obstacle face, the velocities V_i are considered to be proportional to the panels' area, i.e.

$$V = aA \ , \tag{16}$$

where $a > 0$ and A is a column vector with the areas of the panels. The maximum value for a is reached when the convergence condition is set to the limit, i.e., the repulsive nature of the panels equals the attractive nature of the goal. The maximum acceptable value for a is thus

$$a_{\max} = \frac{\lambda_g + A^T P^{-1} W}{A^T P^{-1} A} \ . \tag{17}$$

One can now compute a from a safety ratio r_a defined as

$$r_a = \frac{a}{a_{\max}} \ . \tag{18}$$

Finally, Λ is given by

$$\Lambda = P^{-1}(-r_a a_{\max} A + W) \ . \tag{19}$$

After the choice of U and λ_g and the computation of Λ it is possible to determine the potential at an arbitrary point in space. The symmetric of the gradient of this potential gives the velocity of a fluid particle and provides the velocity reference u for obstacle avoidance purposes. Being u_1, u_2 and u_3 the components of the velocity u,

$$u_1(x_1, x_2, x_3) = -\frac{\partial \phi_u}{\partial x_1} - \frac{\partial \phi_g}{\partial x_1} - \lambda_j \sum_{j=1}^{m} \frac{\partial \phi'_j}{\partial x_1} \ , \tag{20}$$

$$u_2(x_1, x_2, x_3) = -\frac{\partial \phi_u}{\partial x_2} - \frac{\partial \phi_g}{\partial x_2} - \lambda_j \sum_{j=1}^{m} \frac{\partial \phi'_j}{\partial x_2} \tag{21}$$

and

$$u_3(x_1, x_2, x_3) = -\frac{\partial \phi_u}{\partial x_3} - \frac{\partial \phi_g}{\partial x_3} - \lambda_j \sum_{j=1}^{m} \frac{\partial \phi'_j}{\partial x_3} \ . \tag{22}$$

For further details on the computation of these expressions, please refer to Cruz [7]. Please note that the potential field gradient provides the velocity direction and speed of a fluid particle. However, for fixed wing aircraft obstacle avoidance applications, the aircraft speed should be controlled by a different algorithm to prevent the aircraft from stalling. Usually, speed control is left for the autopilot. For these applications, u is used only to compute a reference for the direction of the aircraft velocity vector.

3 Particularization of the Algorithm

This section describes further adaptations of the panel method for obstacle avoidance purposes when fixed wing aircraft are considered.

The panel method was developed to describe the motion of a fluid particle and thus it does not take into consideration the UAV dimensions. Additionally, the ground is not modelled and the UAV can be directed bellow an obstacle or even bellow the ground (negative heights). In order to deal with local maps that are iteratively updated, some of the algorithm parameters must be automatically computed from obstacles information. Finally, the reference for the direction of the velocity vector taken from the potential field must be converted into commands accepted by the Piccolo autopilot. Next subsections tackle all these issues.

3.1 Obstacle Expansion

To avoid the possibility of collision due to the dimension of the UAV, the detected obstacles are expanded. Considering that the detected obstacles are approximated by rectangular prisms, the expansion is carried out by moving the faces outwards by an amount equal to the wingspan b. The minimum value that assured clearance to the obstacle was half span. However, this distance may not be enough in the presence of any source of error. By moving the faces a distance of b, a separation of at least half span to the nearest object is assured, if no disturbance is considered.

To calculate the expansion of a vertex A, vectors v, w and z from B, C and D to A are defined, where B, C and D are the prism vertices adjacent to A (see Fig. 5). The new vertex A' is then given by

$$A' = A + b\left(\frac{v}{|v|} + \frac{w}{|w|} + \frac{z}{|z|}\right) \ . \tag{23}$$

3.2 Extension of Obstacles Relative to the Ground Plane

In order to prevent any situation that places the aircraft in danger, it is desirable that the obstacle avoidance algorithm does not direct the UAV bellow any detected obstacle. One way of

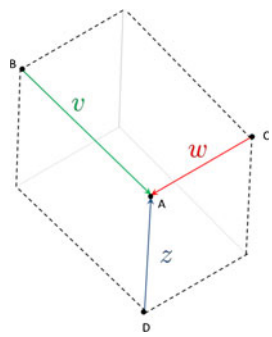

Fig. 5 Vectors to compute the vertices of the expanded obstacle

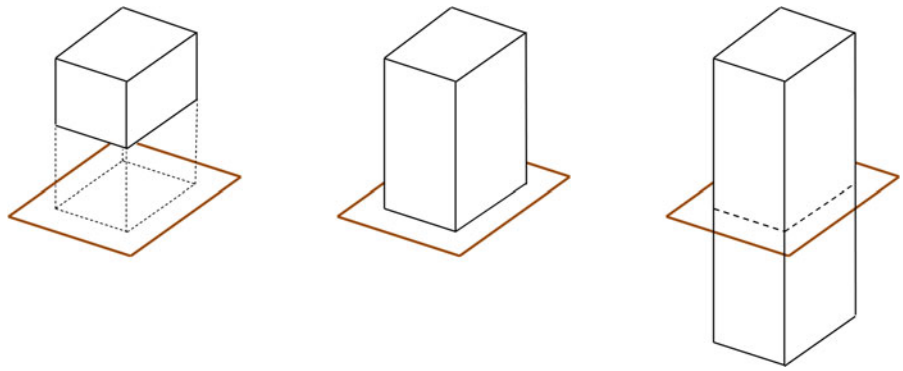

Fig. 6 Obstacle extension to ground plane and extension through the ground plane

accomplishing this is to consider that all obstacles extend to the ground. However, the obstacle avoidance algorithm could even then try to guide the UAV bellow the obstacle (i.e., bellow the ground). Thus, obstacles are further extended creating prisms with an imaginary part bellow ground with the same height that was detected above ground (please refer to Fig. 6).

3.3 Parameter Tuning

As was presented in Section 2, the potential field computation needs some parameters to be set, namely the uniform flow strength (U), the safety ratio (r_a) and the sink strength (λ_g). Depending on these parameters, the UAV will have a different behavior while avoiding the obstacles.

According to the simulations performed, a uniform flow strength $U = 900$ m/s is adequate in the majority of the situations. This value does not have a physical meaning and was obtained experimentally to achieve smooth trajectories. The safety ratio should be selected between 0 and 1, values near 1 implying trajectories farther from the obstacles.

The sink strength λ_g has a strong impact on the panel intensities computation. Higher values of λ_g allow for higher values of the panels intensities λ_j and thus will deviate more the UAV from the obstacles. In a scenario where the number and size of obstacles are unknown a priori and change over time, it is impossible to use a single value for λ_g and expect that the algorithm performs satisfactorily in every situation. In this work, an heuristic formula to automatically compute the sink strength is proposed, making λ_g proportional to the total area of the obstacles as given by

$$\lambda_g = \alpha \sum_{i=1}^{m} A_i \text{ with } \alpha > 0. \tag{24}$$

A value of $\alpha = 100$ was found appropriate for most situations. When no obstacle is detected, λ_g was set to 1,000.

3.4 Autopilot Reference Computation

Formulas (20) to (22) give the components of the velocity vector computed from the potential field (5). As mentioned above, the direction of this velocity vector provides the reference for the UAV velocity vector direction, while the amplitude of the UAV indicated airspeed (IAS) is kept constant by the autopilot. The Piccolo autopilot accepts heading and vertical rate commands [22] that can be used through expressions

$$\psi = \arctan 2\left(\frac{u_1}{u_2}\right) \tag{25}$$

and

$$\dot{h} = \text{IAS}\frac{\hat{u}_3}{\sqrt{\hat{u}_1^2 + \hat{u}_2^2 + \hat{u}_3^2}} \tag{26}$$

to control the UAV velocity vector direction. Since the Piccolo has an hard constraint on the allowed vertical rate values, the vertical rate computed from Eq. 26 is saturated to a maximum absolute value of 3.3 m/s.

Fig. 7 Antex-M X02

4 Simulation Setup and Results

4.1 Simulation Setup

The proposed algorithm was evaluated through hardware in the loop simulations with the ANTEX-M X02 aircraft (Fig. 7). This UAV was built at the Portuguese Air Force Academy with the main characteristics given in Tables 1 and 2.

Figure 8 shows the simulation setup. The UAV dynamics is simulated by the Simulator software provided by Cloud Cap.[1] It receives the commands from the Piccolo autopilot and provides back the UAV state information via a can bus interface. The communication between the Piccolo and the obstacle avoidance algorithm implemented on Matlab® is mediated by the Ground Station, the Piccolo Command Center (PCC) and DUNE, a middleware software developed at the Faculty of Engineering of the University of Porto [20]. The Ground Station is connected to the Piccolo autopilot via an aerial UHF link, receiving the UAV state and transmitting the control references, and to the PC that runs the obstacle avoidance algorithm through a serial cable. From this Ground Station it is possible to monitor in real-time every aspect of the mission. Additionally, at any time a human pilot can take over aircraft control for safety reasons. This setup is very close to real flight operations, in which only the Simulator software is replaced by the actual aircraft and the can bus connection is removed. Figure 9 shows a picture of the experimental setup.

To simulate the obstacle avoidance algorithm, since there's still no obstacle detection system available on the PITVANT aircraft, a simple simulation of such a system was implemented. To be realistic, an obstacle detection system for these applications should only detect obstacles that are within the range of the onboard sensors.

A range finder system was simulated with a beam maximum range of 300 m (see Fig. 10). Beam elevation was varied between −45 and 45°, and beam azimuth between −30 and 30° (see Fig. 10)

Obstacle detection information (heading and distance to the UAV for every beam that intersected an obstacle surface) is used to build a local map of the environment. This map is simply a square occupancy grid, centered at the UAV, with side length of 600 m. Square 20 × 20 m grid cells were considered. Only the obstacle top vertices' information is registered onto the occupancy grid, assigning the value of the obstacle height to the cell corresponding to such a vertex. The cells corresponding to the detected obstacle top edges are filled in by linearly connecting the top vertices. Since it is assumed that the obstacles are rectangular prisms, this 2D grid contains enough information to describe them. The local map is iteratively updated and thus, after some iterations, obstacles correspond to clusters of occupied cells. A rectangle with minimum area that contains each cluster of occupied cells is computed and taken as the top surface of the obstacle, at the height given by the cells values.

The map of the Portuguese Air Force unit where usually PITVANT mission flights take place was used for the algorithm simulation. Three different obstacles configurations, each requiring different avoidance capabilities, are here presented to illustrate the proposed obstacle avoidance system performance.

The first set consists of four separated obstacles (Figs. 11 and 12). The first obstacle has an altitude of 500 m making impractical an avoidance maneuver over it. The second obstacle is 500 m wide and thus should be avoided by flying above it. The third and fourth obstacles have more typical dimensions (300 m and 250 m heights, 200 m

[1] www.cloudcaptech.com

Table 1 Antex-M X02 aircraft main features, fuselage and motor characteristics

	Main features		Fuselage		Motor
Maximum take-off weight	10 kg	Area	0.031 m^2	Model	Saito100, 1.8hp
Wing Span	2.415 m	Length	0.850 m	Mass	0.800 kg
Payload	4 kg		Mass	1.732 kg	
Maximum velocity	150 km/h				
Autonomy	1.5 h				

Table 2 Antex-M X02 main wing and control surfaces dimensions

	Main wing		Horizontal stabilizer	Vertical stabilizer
Airfoil	FX 63-137	Area	0.1184 m^2	0.0403 m^2
Mass	1.468 kg	Span	0.74 m	0.260
Area	0.7848 m^2	Taper ratio	1	0.722
Wingspan	2.415 m	Mass	0.388 kg	0.161 kg
	Ailerons		Elevator	Rudder
Chord	0.043 m	Chord	0.051 m	0.056 m
Area	0.0215 m^2	Area	0.003412 m^2	0.01456 m^2

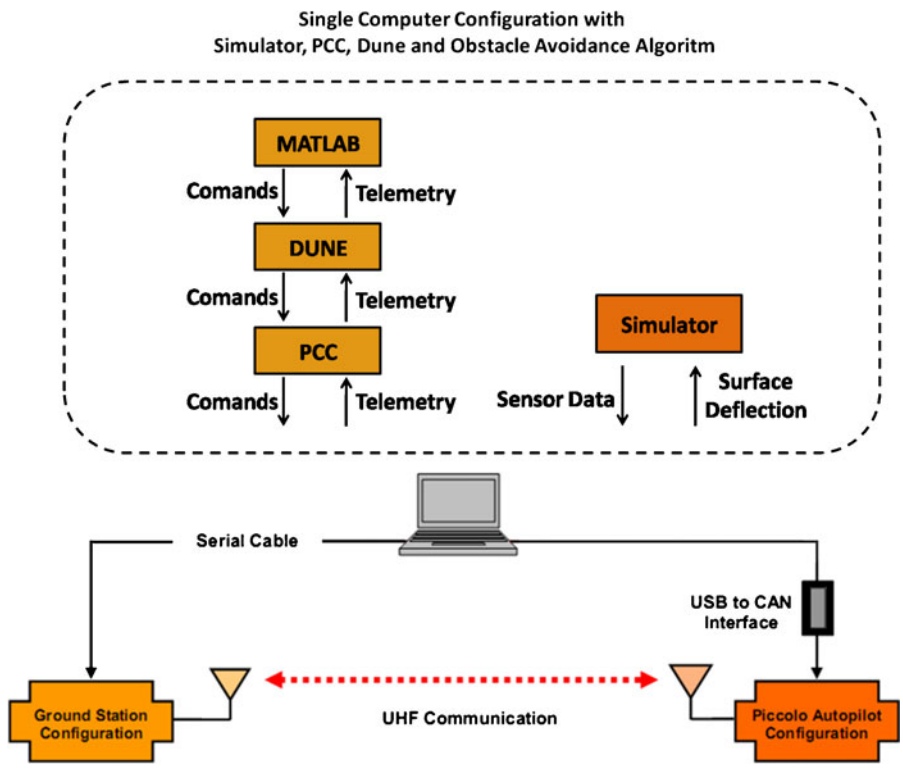

Fig. 8 Control system architecture used in the HIL simulations. Adapted from Piccolo Setup Guide [25]

Fig. 9 Experimental setup used for Hardware-In-Loop simulations

wide). The second set consists of three obstacles with an altitude of 300 m, with two of the obstacles being approximately parallel to the trajectory and the third obstacle overlaps the other two, blocking the way to the UAV's goal (Figs. 15 and 16). In this case, the only way to avoid the obstacles is to pass over the obstacles or to circumvent them. The third obstacle configuration (Figs. 17 and 18) is similar to the second, but the obstacles do not overlap, leaving enough space between them to allow the UAV to pass through, and their altitude is 1,000 m.

The initial flight conditions for the three simulation are: leveled flight with heading 180° and with an altitude of 180 m. The UAV indicated air speed was set to 22 m/s. When the obstacle avoidance algorithm is activated, the UAV's goal is defined to be a point 2,000 m further a line approximately parallel to the airfield taxiway, with an altitude of 150 m. As the first obstacle set is intended to be more realistic, wind (pointing Southwest with an amplitude of $3\sqrt{2}$ m/s) and turbulence disturbances were added.

The global maps were used as inputs to the simulated obstacle detection system. The obstacle avoidance algorithm only relied on the information of a local map of the environment, i.e., on the output of the simulated obstacle detection system.

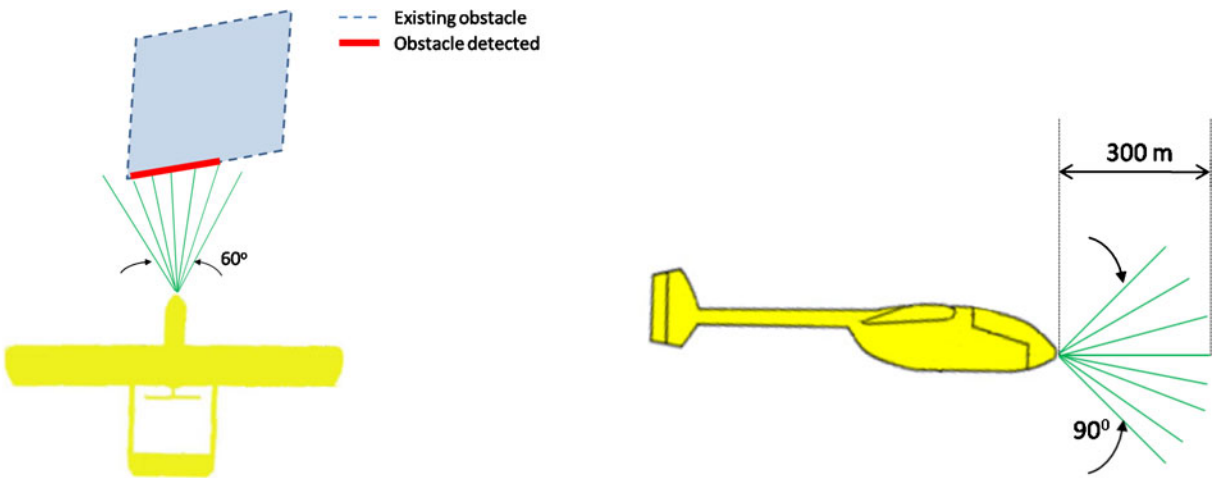

Fig. 10 Simulated range finder diagram

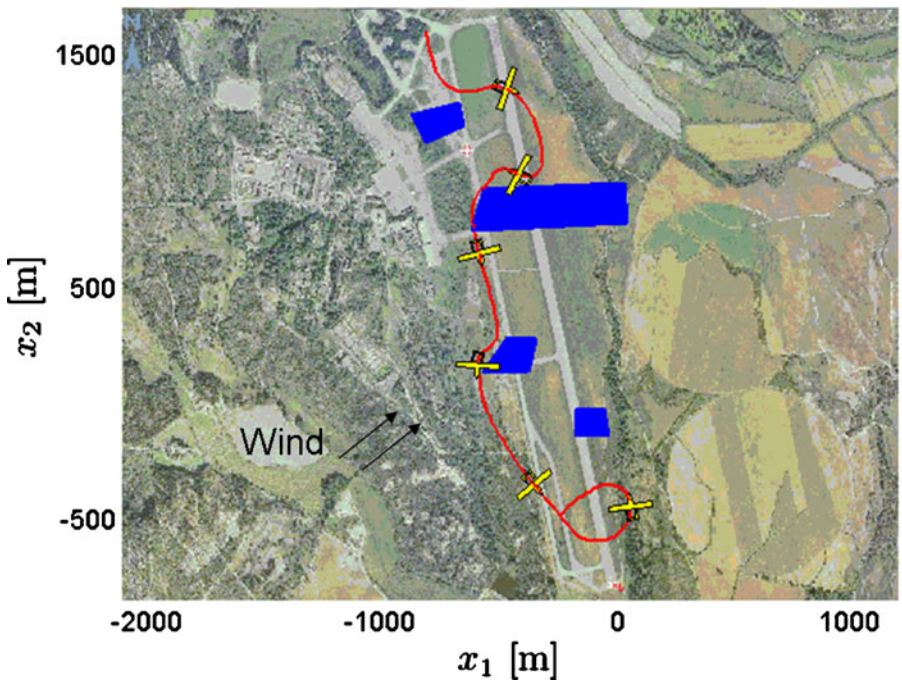

Fig. 11 Top view of the path described by the UAV in the HIL simulation with the first set of obstacles

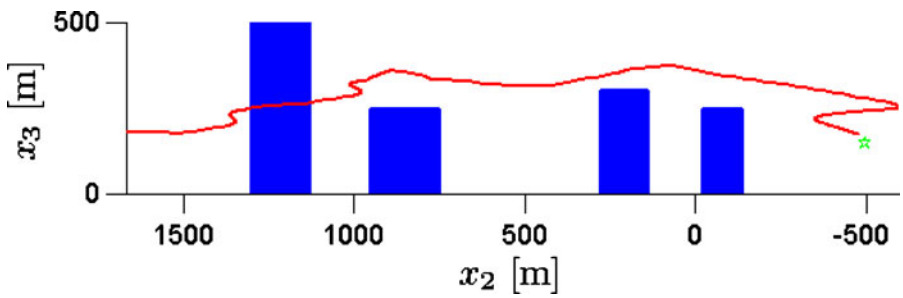

Fig. 12 Side view of the path described by the UAV in the HIL simulation with the first set of obstacles

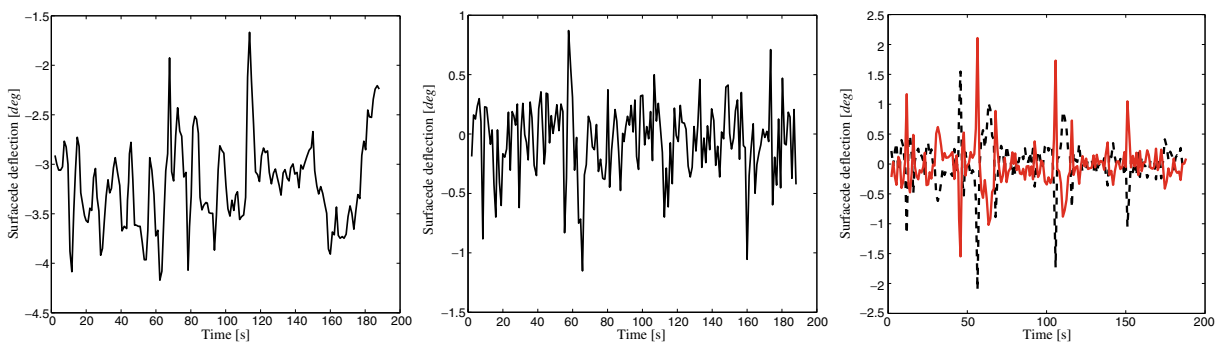

Fig. 13 Elevator, rudder, right (*red continuous line*) and left (*black dashed line*) ailerons deflections during HIL simulation with the first set of obstacles

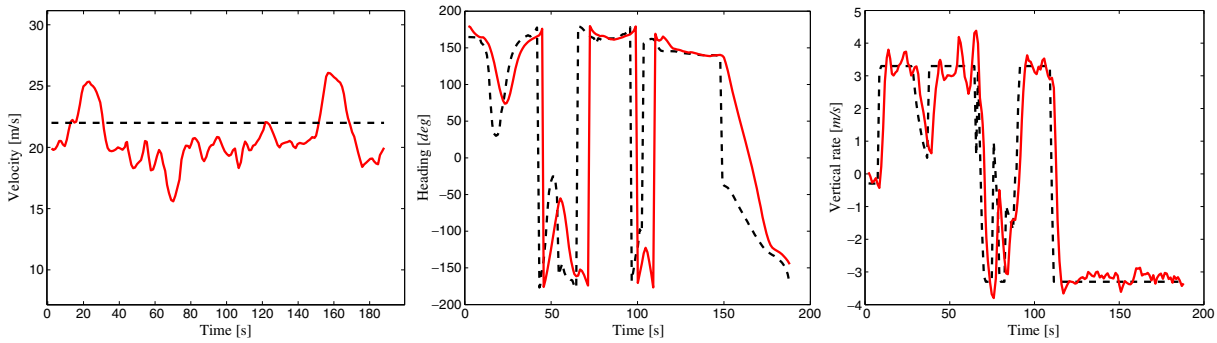

Fig. 14 Airspeed, heading and vertical rate reference command (*black dashed line*) and real value (*red continuous line*) during HIL simulation with the first set of obstacles

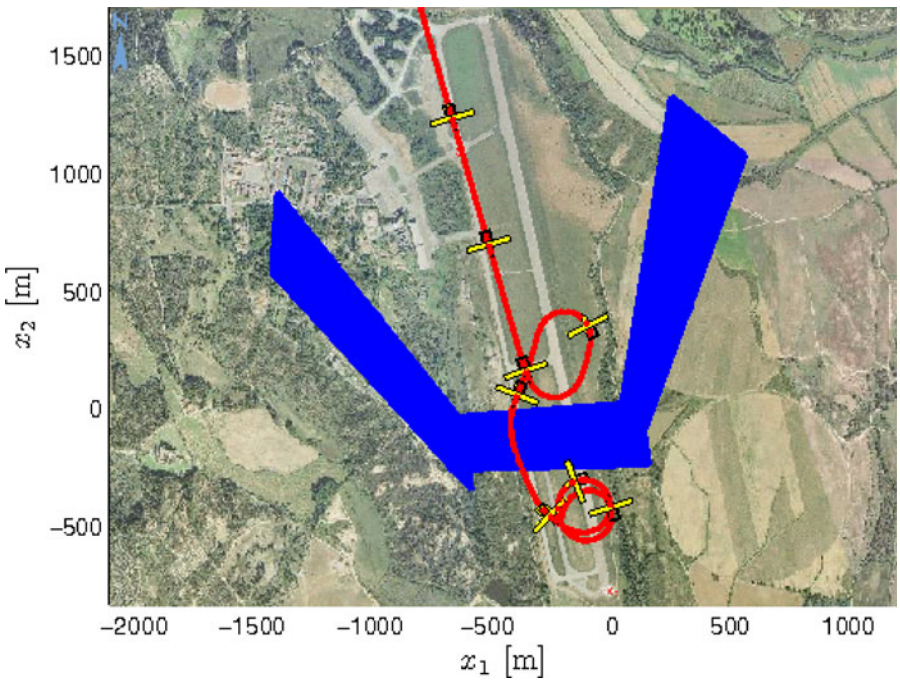

Fig. 15 Top view of the path described by the UAV in the HIL simulation with the second set of obstacles

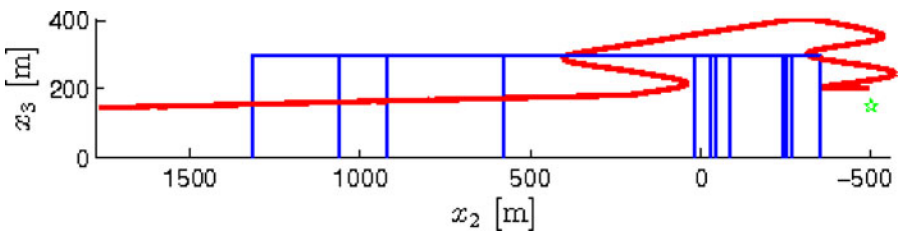

Fig. 16 Side view of the path described by the UAV in the HIL simulation with the second set of obstacles

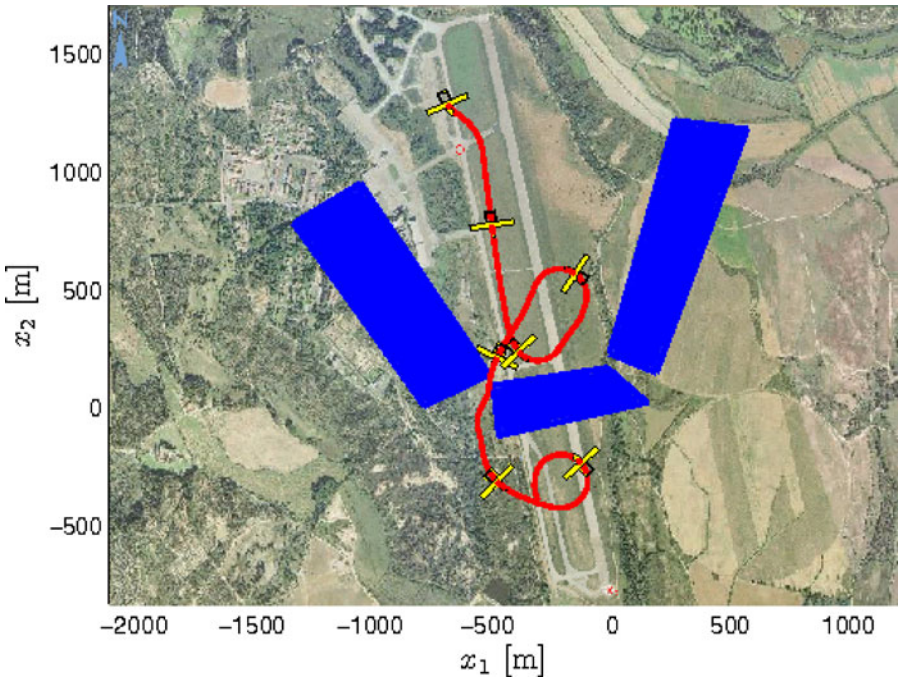

Fig. 17 Top view of the path described by the UAV in the HIL simulation with the third set of obstacles

4.2 Simulation Results

Figures 11, 12, 13, and 14 show the UAV trajectory, the UAV control surface deflections and the UAV airspeed for the first simulation scenario. From Figs. 11 and 12 it is clear that the obstacle avoidance algorithm successfully guided the UAV towards its goal avoiding the obstacles, taking 171 s to go through a path 3,726 m long. Diversion maneuvers included passing beside and above obstacles. After the third obstacle the UAV starts descending to achieve the goal altitude. However, due to the maximum allowed vertical rate, the aircraft reaches the goal point flying higher than it should and thus it has to pass it and perform a loiter-like maneuver, returning to the goal point at the desired altitude.

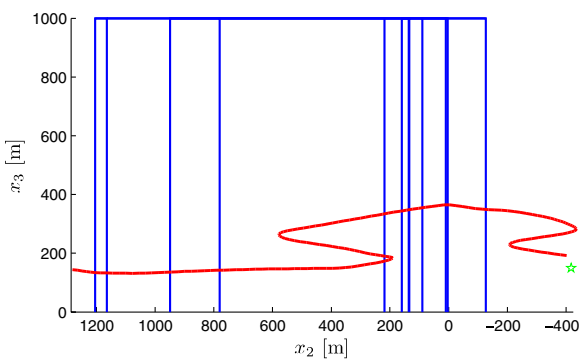

Fig. 18 Side view of the path described by the UAV in the HIL simulation with the third set of obstacles

Control surfaces deflections are depicted in Fig. 13, showing that they stay within admissible values. Figure 14 (left) presents the aircraft airspeed. Airspeed variation is mainly due to the presence of wind and to the Piccolo wind estimators performance. Nevertheless, the UAV's speed always remained well above the stall speed (13 m/s). From Fig. 14 center and right plots, it is noticeable the delay between the reference heading and vertical rate and the actual UAV variables. This is due to the vehicle dynamics. Also it is very clear the vertical rate reference saturation.

In the second simulation scenario (Figs. 15 and 16), when the UAV detects the obstacle in front of it, it is impossible to gain altitude in order to pass over the obstacle within the distance available, and the UAV needs to turn back, always ascending, before facing the obstacle again, now

at a convenient altitude. A loiter-like maneuver is again necessary to descend to the prescribed altitude after crossing the obstacles.

With the third set of obstacles (Figs. 17 and 18), the UAV also turns back in order to be able to gain altitude. However, in this maneuver, the simulated obstacle detection system detects a free space between the obstacles and the UAV is directed through it.

5 Conclusions

The paper presented a 3D obstacle avoidance algorithm based on the panel method to derive a suitable potential field. Adaptations needed for application to the control of fixed wing aircraft were also described. Hardware-In-Loop simulations with realistic mission scenarios showed the validity of the proposed algorithm.

However, no formal proof is provided that the UAV will not collide with any obstacle. In fact, the panel method only assures that the symmetric of the potential field gradient points outwards the obstacles at their faces' centers. It is thus theoretically possible that the velocity field at the periphery of an obstacle face points towards that face. Considering the velocity field proportional to the panel area contributes to prevent this possibility. Additionally, the potential field method provides the reference velocity vector for the UAV, but only the velocity vector direction is used, being the aircraft speed controlled by the Piccolo. Finally, the control algorithm was developed at the kinematic level, not taking into consideration neither the dynamics inner loop controlled by the Piccolo (namely saturation of the control signals), nor the disturbance estimator dynamics included in the autopilot (please refer to Kaminer et al. [15] for methods to tackle these issues).

The obstacle avoidance algorithm here presented will now be included in the mission control system of the PITVANT project aircraft. This system will be responsible for switching on the algorithm when obstacles are detected and for computing a goal position to the UAV depending on the ongoing mission. The mission control system should also monitor the performance of the obstacle avoidance algorithm and dictate a predefined emergency maneuver if a potentially dangerous situation is detected. Future work will include also the integration of the vision system under development within the project. Real flight tests will be performed, firstly with the control algorithm running on a ground station, and then on a PC104 onboard the UAV.

Acknowledgements The authors are in debt to every member of the PITVANT research team, with special relevance to Lieutenant Tiago Oliveira.

References

1. AFA-FEUP: O Programa de Investigação e Tecnologia em Veículos Aéreos Autónomos Não-Tripulados da Academia da Força Aérea. II Série Cadernos do IDN, Instituto de Defesa Nacional (2009)
2. Barraquand, J., Langoois, B., Latombe, J.C.: Numerical potential field techniques for robot path planning. In: Proceedings of the Fifth International Conference on Advanced Robotics, vol. 2, pp. 1012–1017. Pisa, Italy (1991)
3. Borenstein, J., Koren, Y.: The vector field histogram—fast obstacle avoidance for mobile robots. IEEE Trans. Robot. Autom. **7**(3), 278–288 (1991)
4. Brock, O., Khatib, O.: High-speed navigation using the global dynamic window approach. In: Proceedings of the 1999 IEEE International Conference on Robotics and Automation, vol. 1, pp. 341–346. Detroit, MI, USA (1999)
5. Call, B., Beard, R., Taylor, C., Barber, B.: Obstacle avoidance for unmanned air vehicles using image feature tracking. In: Proceedings of AIAA Guidance, Navigation, and Control Conference and Exhibit. Keystone, Colorado, USA (2006)
6. Carvalhosa, S., Aguiar, A., Pascoal, A.: Cooperative motion control of multiple autonomous marine vehicles: collision avoidance in dynamic environments. In: Proceedings of IAV 2010—7th Symposium on Intelligent Autonomous Vehicles. Lecce, Italy (2010)
7. Cruz, G.: Desenvolvimento de estratégias de contorno de obstáculos para veículos aéreos não tripulados. Master's thesis, Academia da Força Aérea (2011)
8. DeMuth, G., Springsteen, S.: Obstacle avoidance using neural networks. In: Proceedings of the (1990) Symposium on Autonomous Underwater Vehicle Technology, pp. 213–215. Washington, DC (1990)
9. Fahimi, F.: Autonomous Robots Modeling, Path Planning, and Control. Springer, New York (2009)
10. Fajen, B., Warren, W.: Behavioral dynamics of steering, obstacle avoidance and route selection. J. Exp. Psychol. Hum. Percept. Perform. **29**, 343–362 (2003)
11. Fodrea, L.: Obstacle avoidance control for the REMUS autonomous underwater vehicle. Master's thesis, Naval Postgraduate School (2002)

12. Fox, D., Burgard, W., Thrun, S.: The dynamic window approach to collision avoidance. IEEE Robot. Autom. Mag. **4**(1), 23–33 (1997)
13. Griffiths, S.: Remote terrain navigation for unmanned air vehicles. Master's thesis, Bringham Young University (2006)
14. Hemminger, D.: Vertical plane obstacle avoidance and control of the REMUS autonomous underwater vehicle using forward look sonar. Master's thesis, Naval Postgraduate School (2005)
15. Kaminer, I., Pascoal, A., Xargay, E., Hovakimyan, N., Chengyu, C., Dobrokhodov, V.: Path following for unmanned aerial vehicles using l1 adaptive augmentation of commercial autopilots. J. Guid. Control Dyn. **33**(2), 550–564 (2010)
16. Khatib, O.: Real-time obstacle avoidance for manipulators and mobile robots. Int. J. Rob. Res. **5**, 90–98 (1986)
17. Lapierre, L., Zapata, R., Lepinay, P.: Combined path-following and obstacle avoidance control of a wheeled robot. Int. J. Rob. Res. **26**, 361–375 (2007)
18. Paim, P., Jouvencel, B., Lapierre, L.: A reactive control approach for pipeline inspection with an AUV. In: Proceedings of MTS/IEEE OCEANS, vol. 1, pp. 201–206. Washington, DC, USA (2005)
19. Scherer, S., Singh, S., Chamberlain, L., Saripalli, S.: Flying fast and low among obstacles. In: Proceedings of the 2007 IEEE International Conference on Robotics and Automation, pp. 2023–2029. Rome, Italy (2007)
20. Sousa, J., Gonçalves, G.: Mixed initiative control of unmanned air and ocean going vehicles: Models, tools and experimentation. In: Proceeding of RTO AVT-146 Symposium Platform Innovations and System Integration for Unmanned Air, Land and Sea Vehicles, 9, pp. 1–14. Florence, Italy (2007)
21. Uzol, O., Yavruccuk, I., Uzol, N.: Collaborative target tracking for swarming MAVs using potential fields and panel methods. In: Proceedings of the AIAA Guidance, Navigation and Control Conference and Exhibit. Honolulu, Hawaii, USA (2008)
22. Vaglienti, B., Hoag, R., Niculescu, M.: Piccolo System User's Guide Software v2.0.4 with Operator Interface (OI). Cloud Cap Technology (2007)
23. Waydo, S., Murray, R.: Vehicle motion planning using stream functions. In: International Conference on Robotics and Automation (2003)
24. Wilton, D.R., Rao, S.M., Glisson, A.W., Schaubert, D.H., Al-Bundak, O.M., Butler, C.M.: Potential integrals for uniform and linear source distributions and polyhedral domains. IEEE Trans. Antennas Propag. **32**(3), 276–281 (1984)
25. Zanmiller, M., Miley, D.: Piccolo Setup Guide. Cloud Cap Technology (2009)